The Nature of the Gamma Dielectric Relaxation in Diglycidyl Ether Bisphenol-A (DGEBA) Based Epoxies

Istebreq A. Saeedi [1*], Nikola Chalashkanov [2], Leonard A. Dissado [3], Alun S. Vaughan [1] and Thomas Andritsch [1]

[1*] Tony Davies High Voltage Laboratory, Department of Electronics and Computer Science, University of Southampton, iahs1f21@soton.ac.uk
[2] School of Engineering, University of Lincoln, NChalashkanov@lincoln.ac.uk.
[3] Department of Engineering, University of Leicester, lad4@le.ac.uk.

Abstract: A γ relaxation dielectric loss peak has been measured in the temperature range 113 -163 K for a series of epoxy resins based on diglycidyl ether bisphenol-A (DGEBA) containing varying amounts of functional network modifier. Analysis of the temperature dependence of the loss peak frequency has shown that the relaxation process can best be described in terms of a thermally assisted tunnelling displacement of a proton, termed activated tunnelling. The parameters derived not only fit the experimental data well, but have a clear physical origin that is shown to be consistent with the network topology as expressed through the glass transition temperature. The maximum temperature for which such behavior is observable has been determined and shown to be consistent with the measurements.

Keywords: Dielectric Relaxation; Gamma Relaxation; Proton Tunnelling; Epoxy Resin; Functional Network Modifiers; Barrier Energy; Vibration Frequency; Glass Transition.

1. Introduction

Epoxy resins (ER) constitute a class of thermosetting polymers that finds uses in many different applications, including as adhesives, matrix polymers in high strength composites and as electrical insulation. While epoxy resins may be divided into cycloaliphatic, phenol-formaldehyde, bisphenol-based classes [1–4], many common ER systems are based upon diglycidyl ethers of bisphenol A (DGEBA). Such materials are often cured through the use of amine or anhydride groups. Both amine and anhydride hardeners are widely used commercially, whereas anhydride-cured materials are favored in certain sectors, including the electrical industry, as a consequence of characteristics such as low shrinkage during curing giving dimensional stability and low energy release during curing, which is important in maintaining isothermal conditions throughout large castings [5].

Modification of ER networks can be achieved through the inclusion of reactive components that become covalently bonded into the molecular architecture. This strategy has been used for tailoring the mechanical properties of ERs, where the additives are termed reactive diluents. For example, this approach has been employed to improve impact performance through the incorporation of reactive diluents based upon hydroxyl-terminated polyesters [12], polyurethane-based systems [13] and liquid crystalline polyurethane-imides [14]. From the electrical perspective, a comparable strategy has been proposed, termed functional network modification, which seeks to exploit the changes in network structure that result from the incorporation of so-called functional network modifiers (FNM) in two ways. First, such an approach enables specific functional groups to be introduced into the network, with the potential that such moieties may act as charge traps that can affect charge transport and the breakdown characteristics of the system. A number of studies have considered such effects with respect to stoichiometric imbalances in anhydride- and amine-cured ERs: while a moderate (~20%) excess of epoxide groups reduces DC conductivity at temperatures below the glass transition temperature (T_g), an excess of amine groups was found to promote conduction [15]; elsewhere, a comparable excess of anhydrides resulted in a pronounced reduction in AC breakdown strength in both the base ER and a nano-filled equivalent [16]. In contrast, an increase in breakdown strength of 10% was seen on incorporating glycidyl 4-nonylphenyl ether into an epoxy network (constant, optimal epoxy/amine stoichiometry) [17], while an increase of twice this magnitude was observed on adding a glycidyl

polyhedral oligomeric silsesquioxane into the same base epoxy system (again, constant, optimal epoxy/amine stoichiometry) [18].

The variations in network topology consequent to the introduction of FNMs have the potential to affect the molecular dynamics of the system. Numerous studies of the dielectric response of ERs have been undertaken and, in general, ionic conduction plus three dipolar loss processes are considered, the latter being termed, α, β and γ, which are conventionally interpreted as follows. Ionic conduction manifests itself at low frequencies and at high temperature (above T_g) within the dielectric spectra and is associated with a process of electrode charging as a consequence of ionic mobility [19]. As the temperature is reduced, the free volume in the system is reduced, such that the motion of large chain segments is inhibited. The dipolar dielectric relaxation process related to the long range co-operative motion of chains at and above T_g is termed the α relaxation [20-22]. Below T_g, the local motion of smaller dipolar units results, first, in the β relaxation which, in epoxies, is generally associated with the local rotational motion of pendant hydroxyl groups relative to the chain backbone, [23-25]. Finally, at yet lower temperatures, the γ relaxation is observed, albeit that its origin is of some dispute, with two potential molecular origins being proposed. First, the epoxy γ relaxation has been ascribed to the presence of unreacted moieties, notably epoxide groups within the system [26-31]; second, it has been related to the local motions of backbone sequences, such as methylene sequences including ether groups [20, 32-36].

Our recent studies set out to re-examine the origins of the dielectric processes described above (i.e. ionic conduction, α, β and γ relaxations), using the strategy of functional network modification as a means of adjusting network topology in a controlled and systematic way. Specifically, in this paper, we report on the effect of two related FNM moieties upon the dielectric γ relaxation in an anhydride-cured model diglycidyl ether of bisphenol A epoxy resin. Subsequently, we extend the concepts presented here to the higher temperature relaxations and to other systems, results that will be reported in due course.

2. Experimental

2.1 Materials

The base epoxy resin used in this study was a diglycidyl ether of bisphenol-A (DGEBA), commercially known as DER 332, which was purchased from Sigma Aldrich (CAS-No: 25068-38-6, molar mass: 384.6 g/mol). This bifunctional monomer was used in conjunction with two monofunctional epoxy-terminated functional network modifiers (FNM), namely, glycidyl hexadecyl ether (GHE) and glycidyl 4-nonylphenyl ether (GNPE), also obtained from Sigma Aldrich. The chemical structure of each of these compounds is shown in Figure 1. The manufacturer's quoted epoxide equivalent weight (EEW) of DER 332 is 172-176 g mol^{-1}, while the EEW of GHE and GNPE is, respectively, 298.50 g mol^{-1} and 276.41 g mol^{-1}. The resin was cured using Aradur HY 925 (supplied by Huntsman), which is composed of methyltetrahydrophthalic anhydride (CAS-No: 11070-44-3 – molar mass: 153.8 g mol^{-1}) combined with a trichloro(N,N-dimethyloctylamine)boron amine complex initiator (BCl3:DMOA, CAS-No: 34762-90-8). In all the systems considered here, the stoichiometry was calculated to ensure a constant ratio of anhydride to epoxy groups. Previously, we examined stoichiometry effects in a comparable epoxy/anhydride system to that used here, concluding that a 1 :1 molar ratio of epoxide to anhydride groups is optimal, within experimental uncertainties [37, 38]. The material that does not contain any FNM is hereafter termed the reference system. The systems containing the FNM are referred to as XAGHE or XAGNPE, where X represents the percentage of epoxide groups in the system that was derived from the indicated FNM, A signifies anhydride curing and, GHE or GNPE indicates the appropriate FNM. The various formulations used are listed in Table 1.

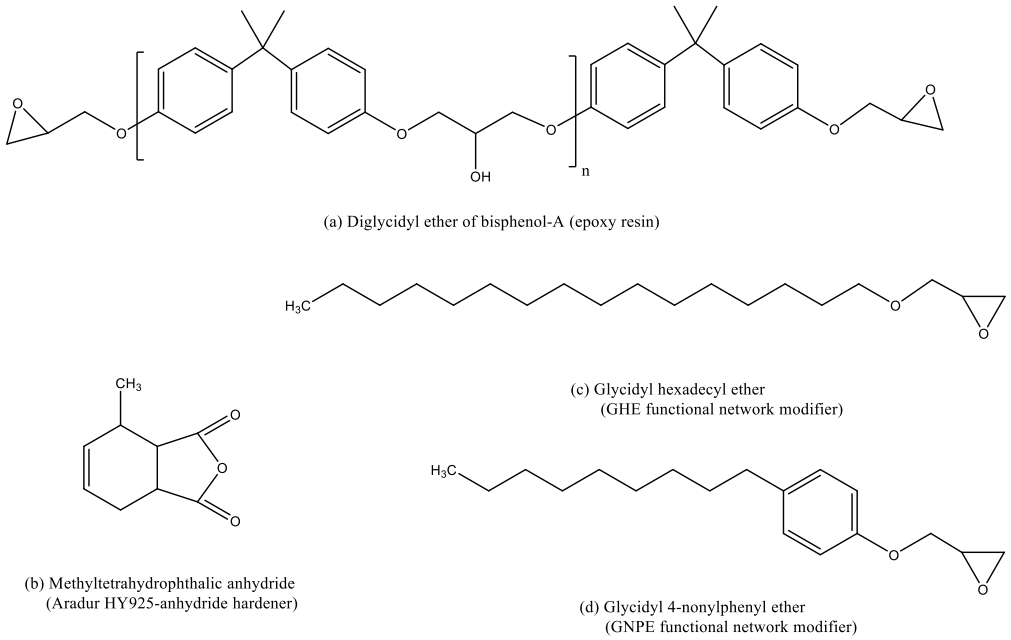

Figure 1. The chemical structure of the resin, hardener and functional network modifiers used in this study.

Table 1. Composition of the four systems considered in this study

Material System	Epoxy Resin / g	Hardener / g	FNM / g
Reference	5.13	4.87	0
30AGHE	3.21	4.45	2.34
20AGHE	3.79	4.6	1.61
30AGNPE	3.26	4.53	2.21

2.2 Sample Preparation

To fabricate the required samples, the resin was first preheated at 323 K for 1 h, to reduce its viscosity, before the required masses of resin and FNM were combined and mixed together using a magnetic stirrer. After 5 min of mixing, the appropriate mass of the anhydride hardener was added to the mixture and the mixing continued for another 5 min. Then, the three-component mixture was degassed in a vacuum oven until no bubbles could be seen in the material and introduced into preassembled steel molds with the required dimensions. All samples were cured in a fan oven using the following two-step protocol. First, they were held at 363 K for 2 h, in order to allow the anhydride initiation reaction to take place, before the temperature was increased to 423 K and held for a further 4 h to complete the curing reaction. The resulting samples were finally removed from the molds and stored under vacuum until use. This is consistent with recommended protocols for comparable commercial systems and was derived from a prior optimization study [38].

The samples so produced were nominally 200 μm in thickness and, for electrical characterization, were gold sputtered with opposing circular electrodes, 20 mm in diameter, to ensure good contact between the test cell electrodes and the sample surface.

2.3 Material Characterisation

The glass transition temperature, T_g, of the various samples was measured by differential scanning calorimetry (DSC), using a Perkin Elmer DSC7 instrument after calibration with high purity indium. For each epoxy system, the thermal behavior of specimens ~10 mg in mass was recorded over two successive heating cycles, in order to erase the prior thermal history of each sample. Each heating scan was conducted from 303 K to 443 K with a cooling scan between the two heating cycles. The heating/cooling rate was kept constant at 10 K min^{-1} throughout the experiment. The data reported here all originate from the second heating scan.

Dielectric data were acquired using a Schlumberger SI 1260 impedance/phase gain analyzer, connected to a Solartron 1296 dielectric interface system. A Janis Research STVP-200-XG cryostat sample holder system was used to control the sample temperature. In this way, it was possible to acquire dielectric spectra over the frequency range of 0.1 Hz to 0.1 MHz from 113 K to 453 K. The applied AC voltage was 1 V peak-to-peak throughout.

3. Results

3.1 Differential Scanning Calorimetry

The effect of changes in molecular composition on network architecture was, initially, examined by DSC; the observed variations in the DSC T_g are indicated in Table 2. From this, it is evident that the inclusion of either monofunctional FNM lowers T_g, and that for systems containing the same molar content of FNM, the presence of GHE results in a larger reduction in T_g than does GNPE. That is, the glass transition temperature of 20AGHE (323 ± 2 K) and 30AGNPE (325 ± 2 K) are equivalent, within experimental uncertainties, while that of 30AGHE was measured, by DSC, as 309 ± 2 K. This final figure is, however, close to the operating limits of our DSC and is therefore best considered as representing an upper limit.

The glass transition temperature of highly crosslinked network polymers such as the epoxy resins considered here is determined by three factors: the crosslink density in the system; the free volume present; the stiffness of molecular segments between network nodes.

Each molecule of DER 332 can be considered to contain two epoxides plus, on average, a small fraction of one hydroxyl group while the anhydride hardener behaves as a bifunctional monomer. As such, substitution of epoxide groups from DGEBA with epoxide groups from either GHE or GNPE – which are only able to react through their single terminal epoxide group – will directly serve to reduce the crosslink density within the system. However, this cannot be the only factor at play, since the depression in T_g in 30AGHE is greater than that seen in 30AGNPE where, in both cases, the same extent of epoxy substitution has occurred. As such, we suggest that the molecular structure of the FNM is also important; here, the alkyl chain in GHE contains sixteen carbon atoms while that in GNPE contains only nine. Consequently, additional free volume should be introduced by the GHE, which is consistent with published work on the effect on T_g of GHE [17] and of FNMs with long chain alkyl groups [39]. Secondly, the GNPE contains an aromatic ring within its chemical structure, which may interact physically with the aromatic rings within the backbone of the epoxy network, thereby restricting the mobility of the overall branching moiety. This process is consistent with the effect of aromatic structures on both the thermal stability of epoxy resins [2] and on T_g [40].

Table 2. Effect of resin composition on DSC glass transition temperature

Sample ID	T_g (°K)
Reference	375 ± 2
30AGHE	309 ± 2
20AGHE	323 ± 2
30AGNPE	325 ± 2

3.2 The Dielectric Gamma Relaxation

Figure 2 presents imaginary relative permittivity data obtained from all four of the systems considered here, acquired at temperatures from 113 K to 163 K i.e. within the temperature range commonly associated with the dielectric γ process in DGEBA-based epoxy resins [41, 42]. The four plots reveal peaks in ε_r'' that, for all formulations, fall within the frequency range 1 – 10 Hz at 113 K. Increasing the temperature results in a progressive increase in the measured values of ε_r'' and a displacement of the peak maximum to higher frequencies; with an extent varying from system to system. Figure 3 compares the form of each system's γ relaxation at 113 K and at 153 K. This latter temperature was chosen since the behavior of the reference system in particular reveals evidence of the β relaxation moving into the considered frequency range at temperature ≥ 153 K, which manifests itself as an increase in ε_r'' with decreasing frequency below ~1 Hz. At the lower temperature, Figure 3a, the γ relaxation in the reference system is characterized by a peak, maximum at ~10 Hz, while both 30AGHE and

30AGNPE exhibit comparable peak shapes, albeit with peak maxima close to 1 Hz. The γ relaxation in 20AGHE is rather different in that, while the peak maximum also falls close to 1 Hz, it appears to be accompanied by a shoulder ranging from ~100 Hz to ~1000 Hz. Significant variations in peak shape are also evident in the data acquired at 153 K, Figure 3b. In the case of the reference epoxy, the shape of the γ relaxation peak at 153 K appears equivalent to that seen at 113 K, but with the peak maximum displaced from ~10 Hz to approaching 100 Hz. In contrast, the shape of the 30AGNPE γ relaxation peak at 153 K is very different from that seen at 113 K. In all cases the peak maximum value of ε_r'' increases with increasing temperature, see Figure 2, in line with previously reported behavior [43]. The behavior of the different formulations is evaluated in the following sections using a master curve approach to identify and quantitatively analyze significant variations.

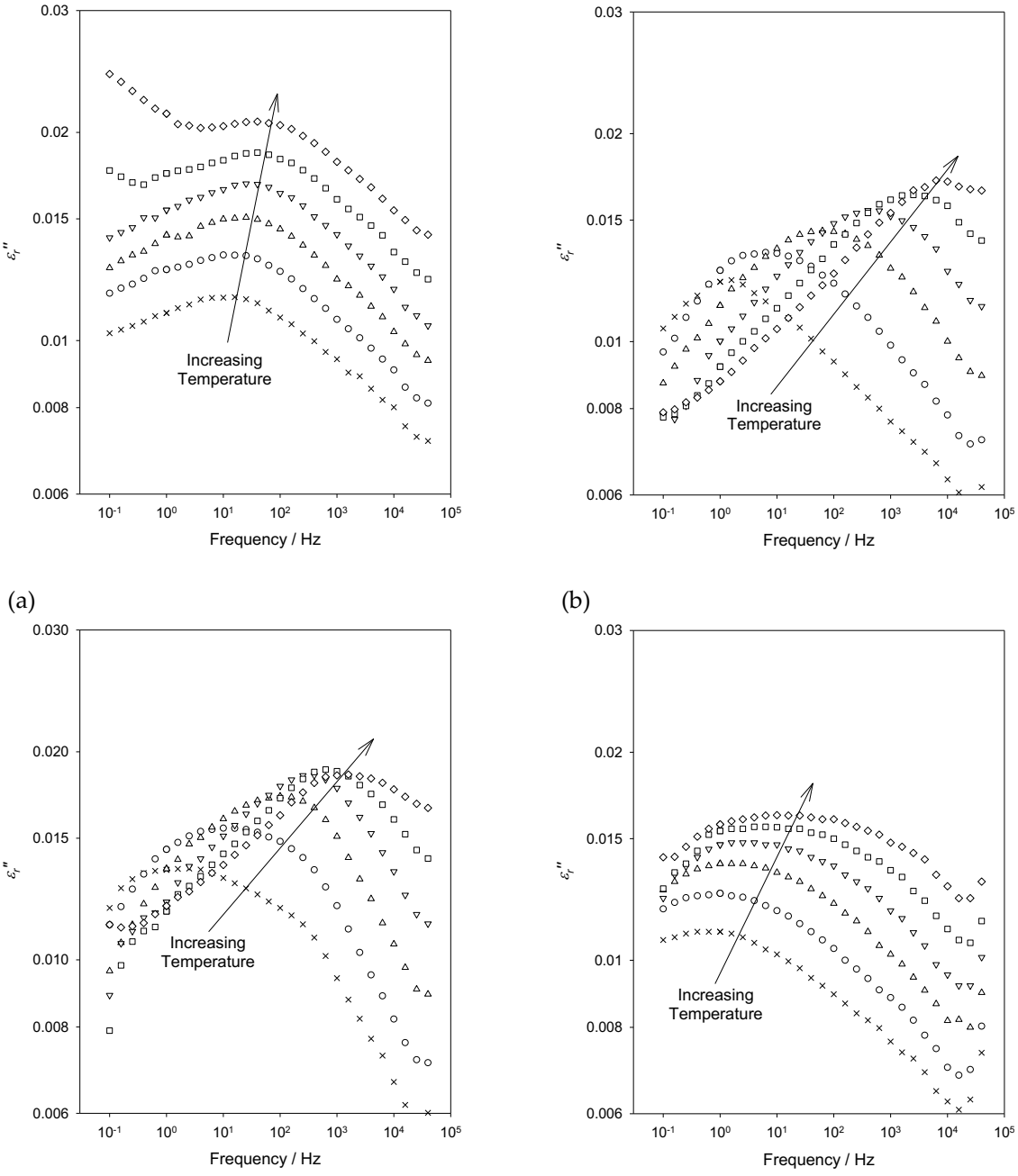

Figure 2. Effect of composition on the frequency dependence of the imaginary part of the relative permittivity, ε_r'': (a) reference epoxy; (b) 30AGHE; (c) 20AGHE; (d) 30AGNPE. In each case the data shown were acquired at the following temperatures: ×113 K; ○123 K; △133 K; ▽143 K; □153 K; ◇163 K.

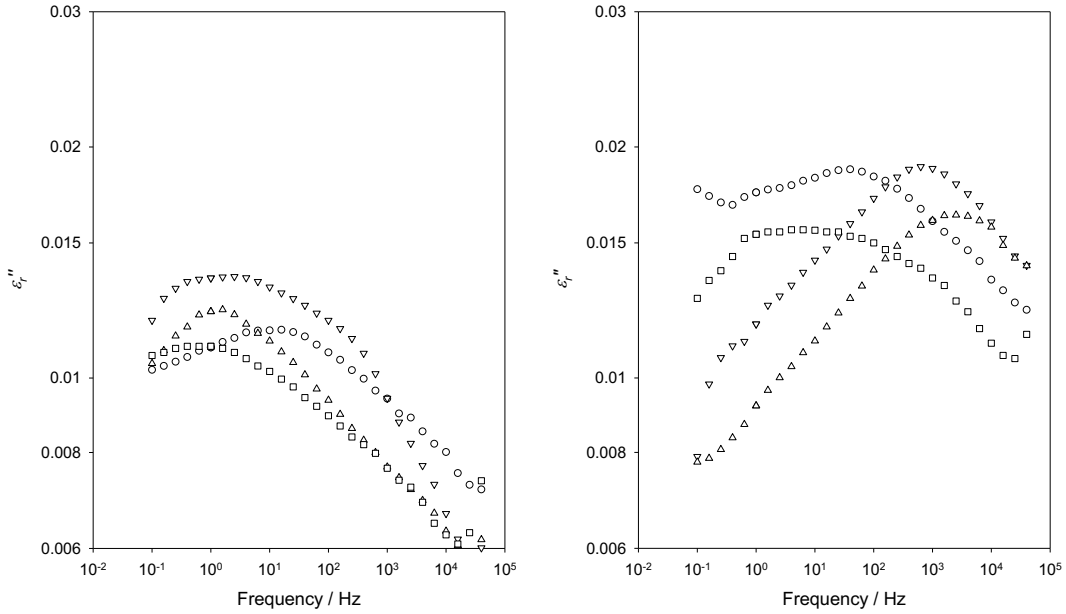

(a) (b)

Figure 3. Plots of the frequency dependence of the imaginary part of the relative permittivity, ε_r'', comparing the behaviour of the formulations at (a) 113 K and (b) 153 K: ○ reference epoxy; △ 30AGHE; ▽ 20AGHE; □ 30AGNPE.

Reference Epoxy System

The master curve for the reference epoxy, Figure 4, demonstrates that the data obtained at different temperatures exhibit the same frequency dependence. The relationship to the characteristic frequency of the reference curve has been moved to the figure caption in this and the following sub-sections. Such data have commonly been analyzed assuming an Arrhenius behavior:

$$f_p = A_0 exp\left(-\frac{E_a}{kT}\right)$$

where f_p is the loss peak frequency, E_a represents the Arrhenius activation energy, A_0 is a constant, T is the absolute temperature and k is the Boltzmann constant.

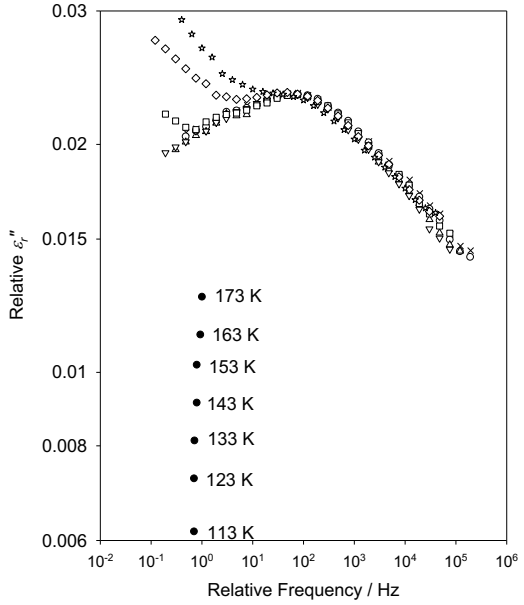

Figure 4. Plots for the reference epoxy system γ relaxation, generated from the imaginary relative permittivity data shown in Figure 2a: × 113 K; ○ 123 K; △ 133 K; ▽ 143 K; □ 153 K; ◇ 163 K; ⋆173 K. The relative shift in frequency and the relative shift in ε_r'' at each of the indicated temperatures are represented by ●.

In line with this, ln f_p is plotted against 1/T in Figure 5a, which leads to an activation energy, E_a, of 0.048 ± 0.005 eV (see Table 3); the quoted uncertainty bounds in this and other parameters were derived from standard error values obtained from the indicated fitted line. Published values for the Arrhenius activation energy of the γ relaxation of epoxy resins commonly range from 0.1 eV to 0.4 eV [27, 43, 44] and have been associated with a number of different molecular entities, including unreacted chain ends [26] and, notably, unreacted epoxide groups [27], and the thermally activated motion of chain segments. In [45] the γ relaxation was related to motion of main-chain sequences of methylene groups, while in [35] it was related to polar ether linkages within the chain structure. However, while [33] ascribed the γ relaxation to main chain ether segments, evidence was also reported for an additional secondary process, which was proposed as being related to residual, unreacted epoxide groups: i.e. chain end moieties. The existence of multiple processes in the γ relaxation region of the dielectric spectrum was also suggested in [27] where a feature termed the δ mode was reported, in addition to an epoxide-related γ mode. Recently, a study of stoichiometry effects in a related series of anhydride-cured epoxy resins based upon the same DGEBA-based epoxide pre-polymer used here similarly reported evidence of two contributions to the γ relaxation, which were termed γ1 and γ2 [38].

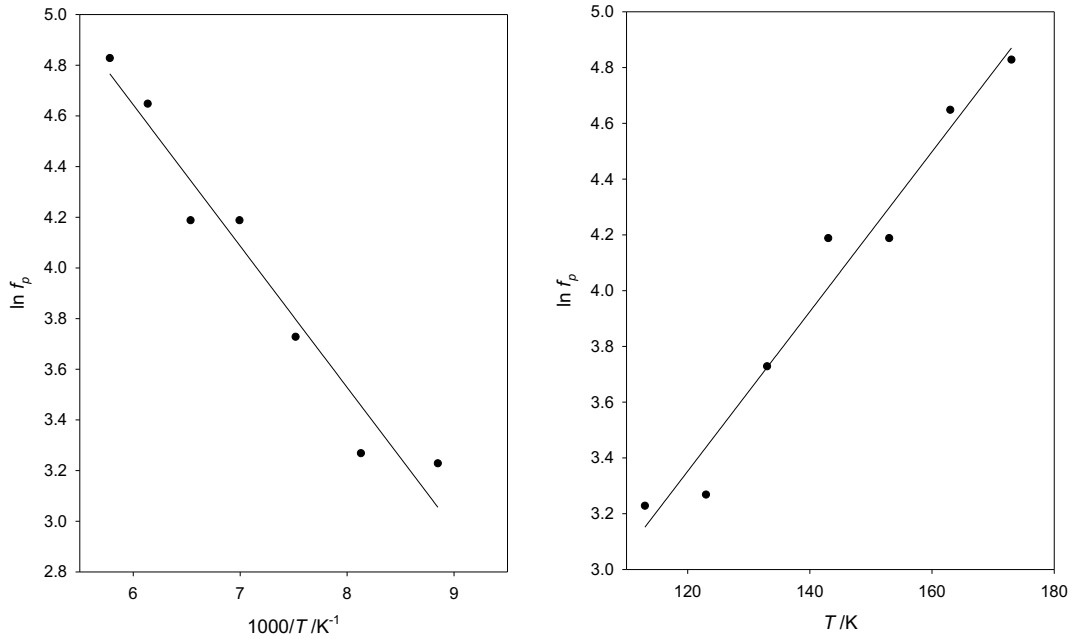

(a) (b)

Figure 5. Analysis of the temperature dependence of the reference epoxy system γ relaxation frequency: (a) Arrhenius plot of lnf_p versus 1/T; (b) activated tunnelling plot of lnf_p versus T.

In this work, γ1 was found to dominate in the reference epoxy resin, was typically observed in the frequency range 1 – 10 Hz, was related to main-chain moieties and, was characterized by an Arrhenius activation energy around 0.07 eV. In contrast, γ2 was observed at higher frequencies (kHz and above) and, being strongly dependent on system stoichiometry, was ascribed to unreacted branch/chain-end dipoles. This process was suggested to be characterized by an Arrhenius activation energy ~0.3 eV when the dominant unreacted moieties were epoxide groups. Here, the activation energy of the characteristic frequency of the γ -relaxation obtained using the Arrhenius approach (i.e. E_a = 0.048 ± 0.005 eV) is somewhat lower than values found in the literature for similar systems. The Arrhenius analysis portrayed in Figure 5a also leads to the evaluation of the pre-exponential term, A_0, which in this case, has a value of 3000 ± 1200 Hz. In chemical reaction kinetics, the Arrhenius A_0 factor can be envisaged as a collision frequency and, as such, may be considered as an attempt frequency which, within the context of the processes considered here, should be related to the vibrational behavior of the relevant

structural unit. In the case of macromolecular systems, the so-called fingerprint region of the infra-red spectrum and terahertz spectra are associated with the cooperative motion of chain segments and, as such, it is to be expected that derived values for A_0 should be in the THz range, not the kHz range seen here. This discrepancy indicates that while the Arrhenius equation may provide an adequate mathematical *description* of the temperature dependence of the γ relaxation process, its physical interpretation is problematical here.

Hill and Dissado [46] have previously considered the temperature dependence of relaxation mechanisms in solids and contrasted thermally activated relaxation processes with mechanisms that involve quantum mechanical tunnelling through a potential barrier, where Δ represents the height of the potential barrier, either side of which lie potential energy minima separated by a distance d_0. Of specific relevance to the data presented above, they discussed [46] the concept of multi-phonon relaxation involving tunnelling relaxation between pairs of higher vibrational levels, energy E_v, within the double minima system, such that the height of the potential barrier above the relevant excited states is reduced to (Δ - E_v) and their spatial separation is reduced to ΔR. This process they termed activated tunnelling and showed that the optimum relaxation rate, f_p, can then be written:

$$f_p = f_t exp\left(\frac{2}{15}A^2 d_0^2 kT\right)$$

where A and f_t are constants. Furthermore, the constant A can be written:

$$A = 4\pi(2m^*)^{1/2}h^{-1}$$

where m^* is the effective mass of the relevant tunnelling particle and h is Plank's constant; the zero temperature rate constant, f_t, is then written:

$$f_t = f_0 exp\left\{-Ad_0\left(\frac{8\Delta}{15}\right)^{1/2}\right\}$$

where f_0 is the vibration frequency of the particle at the energy minima which, for the double minima system of the model, is given by:

$$f_0 = \frac{2}{\pi}\left(\frac{2\Delta}{m^* d_0^2}\right)^{1/2}$$

Analysis of the temperature dependence of f_p therefore directly yields the value of d_0 and f_t. Use of the expression giving f_0 in terms of d_0 and Δ together with the experimental value of f_t then allows both Δ and f_0 to be evaluated.

Specifically, this analysis considered experimental data obtained from a number of polymeric systems, demonstrated a linear temperature dependence of the log of the relaxation rate with T and, showed that if the relevant particle were assumed to be characterized by a hydrogenic proton mass, then this leads to values of Δ in the range 0.31 – 0.65 eV and d_0 values of 0.2 – 0.25 nm in all four of the polymers considered. As pointed out, d_0 values in the above range for protonic masses are consistent with the rotation around C-C bonds. Following this approach, ln f_p is plotted against T in Figure 5b, which demonstrates a good linear relationship between these quantities. Implementing the specific interpretation described above leads to values for f_0, and Δ of 68 ± 5 THz and 0.77 ± 0.05 eV respectively, Table 3. Unlike for the thermally activated Arrhenius analysis portrayed in Figure 5a, both of these values are physically reasonable.

Table 3. Derived parameters

System	Arrhenius		Activated Tunnelling		
	A_0 / *THz*	E_a / *eV*	Frequency / THz	Δ / *eV*	d_0 / *Å*
Reference	(1 – 3) x 10^{-9}	0.048 ± 0.005	68 ± 5	0.77 ± 0.05	1.14 ± 0.05
30AGHE	0.4 – 7	0.271 ± 0.002	17.4 ± 0.4	0.304 ± 0.001	2.8 ± 0.1
20AGHE	(2 – 8) x 10^{-5}	0.146 ± 0.008	25.35 ± 0.01	0.3462 ± 0.00001	2.044 ± 0.001
30AGNPE	(7 – 160) x 10^{-6}	0.18 ± 0.02	26.4 ± 0.9	0.380 ± 0.002	2.1 ± 0.1

30AGHE

The γ relaxation master curve generated for the 30AGNE system is presented in Figure 6. Reference to the characteristic frequency of the reference curve is in the figure caption. As in Figure 4, these results also evince excellent correspondence between the data obtained at different temperatures and, for consistency with the above discussion, quantitative analysis was undertaken using both the Arrhenius equation and according to the activated tunnelling theory [46].

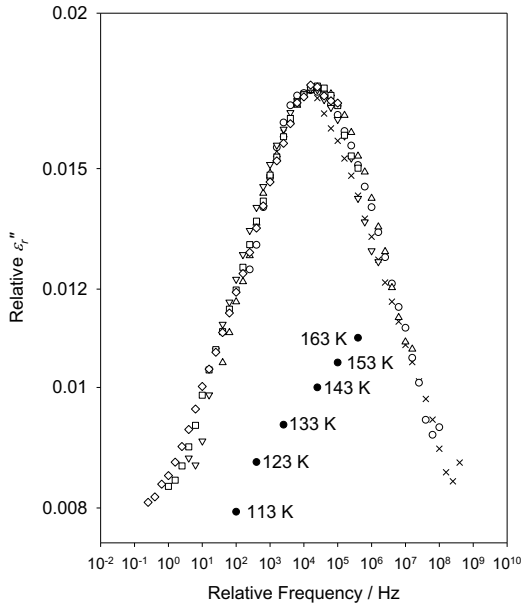

Figure 6. Master plot for the 30AGHE epoxy system γ relaxation, generated from the imaginary relative permittivity data shown in Figure 2b: × 113 K; ○ 123 K; △ 133 K; ▽143 K; □153 K; ◇163 K. The relative shift in frequency and the relative shift in ε_r'' at each of the indicated temperatures are represented by ●.

Equivalent plots to those of Figure 5 for the reference system are shown in Figure 7 for 30AGNE, from which it is evident that plotting ln f_p against both $1/T$ and T leads to linear dependencies and, therefore, both approaches well describe the experimental data. The Arrhenius plot for 30AGNE gives values for the pre-exponential A_0 parameter that fall in the range 0.4 – 7 THz and an activation energy of 0.271 ± 0.002 eV – values that are markedly different from those found in the reference epoxy system. Indeed, as discussed above, this value for E_a is consistent with published Arrhenius activation energy values for epoxy-based systems [27, 43, 44], while the pre-exponential A_0 parameter is physically reasonable, falling as it does in the THz frequency range and therefore being consistent with the vibrational frequencies of chain segments. The activated tunnelling analysis, Figure 7b, leads to values

of f_0, and Δ of 17.4 ± 0.4 THz and 0.304 ± 0.001 eV respectively (see, Table 3), which, unlike in the case of the reference system, are in line with results obtained from the Arrhenius plot.

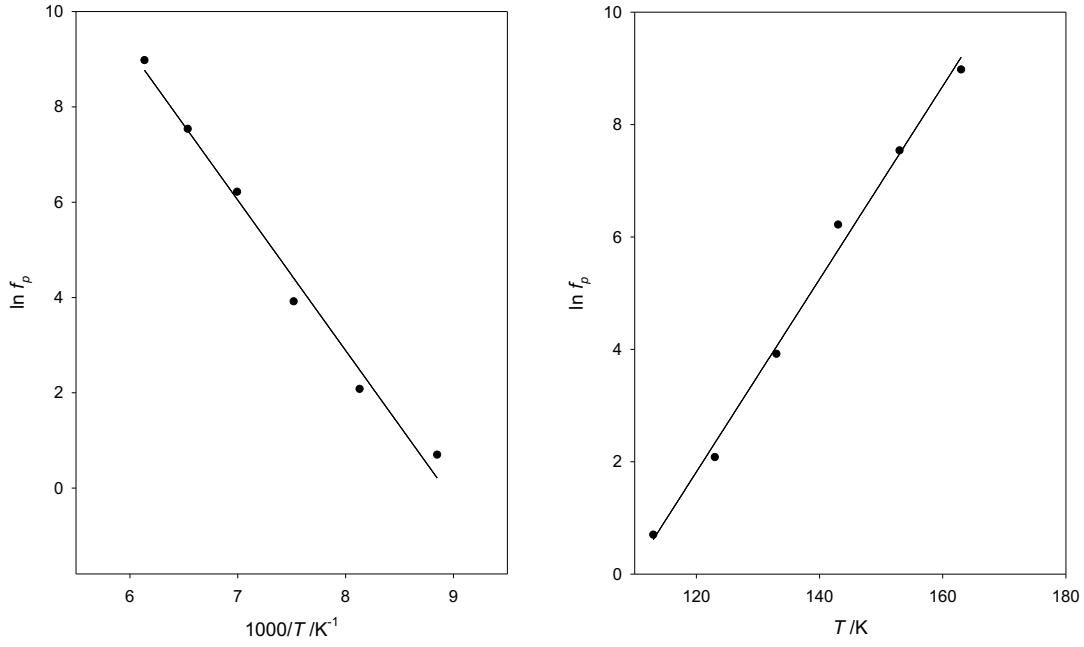

(a) (b)

Figure 7. Master Analysis of the temperature dependence of the 30AGHE system γ relaxation frequency: (a) Arrhenius plot of lnf_p versus 1/T; (b) activated tunnelling plot of lnf_p versus T.

20AGHE

Figure 8 shows the γ relaxation master curve generated for the 20AGHE system. Reference to the characteristic frequency of the reference curve is in the figure caption. Compared to the previous two systems, correspondence between the data sets obtained at the different temperatures is less good in this case, as a consequence of variations in the peak shape at lower temperatures. While excellent correspondence is evident at temperatures above 133 K, below this temperature, the peak becomes increasingly broadened.

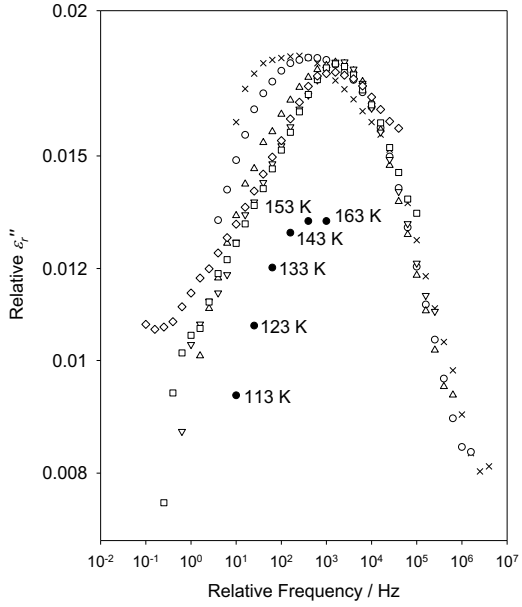

Figure 8. Master plot for the 20AGHE epoxy system γ relaxation, generated from the imaginary relative permittivity data shown in Figure 2c. × 113 K; ○ 123 K; △ 133 K; ▽ 143 K; □ 153 K; ◇ 163 K. The relative shift in frequency and the relative shift in ε'' at each of the indicated temperatures are represented by ●.

Figure 9 shows the derived peak frequencies plotted according to the Arrhenius and activated tunnelling approaches. Comparison of these two plots shows that while the data correspond extremely well to the latter model, correspondence with the Arrhenius equation is relatively poor in that, when ln f_p is plotted against $1/T$, the data appear to fall on a curve rather than being scattered randomly around the best fit line. This issue may be related to some experimental error in the data acquired from this sample at low temperature, where the shape of the relaxation peak appears to vary. Alternatively, the variation in the peak shape may be genuine, leading to uncertainty in evaluating the correct peak shift, which would feed through into an error in the value of f_p. Nevertheless, the R^2 value for this plot is still acceptably high at 0.9884 and, therefore, the Arrhenius A_0 and E_a values were evaluated using the fit shown, leading to values of 20 – 80 MHz and 0.146 ± 0.008 eV respectively. In contrast, the activated tunnelling approach, Figure 9b, shows an excellent linear dependence when ln f_0 is plotted against T; the indicated line equates to an R^2 value of 1.0000 and leads to values of f_0 = 25.35 ± 0.01 THz and Δ = 0.3462 ± 0.00001 eV (Table 3).

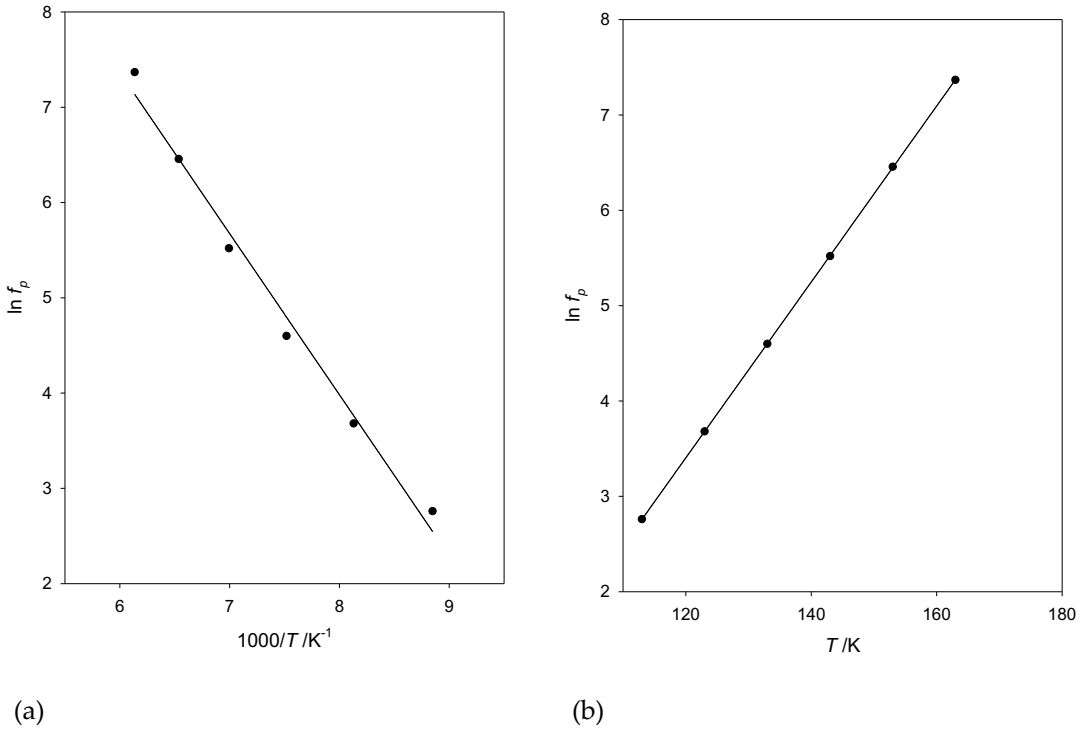

Figure 9. Analysis of the temperature dependence of the 20AGHE system γ relaxation frequency: (a) Arrhenius plot of lnf_p versus $1/T$; (b) activated tunnelling plot of lnf_p versus T.

30AGNPE

The γ relaxation master curve for the 30AGNPE system is shown in Figure 10, which again reveals excellent correspondence between the data acquired at most temperatures, albeit that a degree of deviation is evident below the peak maximum in the case of the data acquired at the two highest temperatures, 153 K and 163 K, presumably, as a consequence of the β relaxation moving into the accessible frequency range. The derived characteristic frequency values are plotted in the form of ln f_p versus $1/T$ and T in Figures 11a and 11b respectively. It is evident that this Arrhenius plot, Figure 11a, is characterized by a high degree of curvature; this is comparable in form to that seen in Figure 9a, but much more marked (R^2= 0.9204). Values of A_0 and E_a determined from the best fit line to the complete data set are presented in Table 3. However, in view of the possible perturbing influence of the β relaxation implied by the variation in peak shape evinced by Figure 10, it may be argued that the characteristic frequency values acquired from this material at the two highest temperatures are unreliable but, even neglecting these two data points, the remaining data are still not scattered about a straight line.

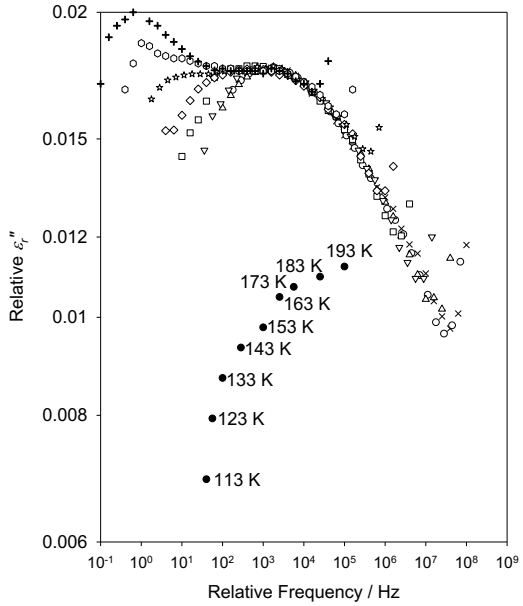

Figure 10. Master plot for the 30AGNPE epoxy system γ relaxation, generated from the imaginary relative permittivity data shown in Figure 2d: × 113 K; ○ 123 K; △ 133 K; ▽ 143 K; □ 153 K; ◇ 163 K; ⋆173 K; ⬡ 183 K; + 193 K. The relative shift in frequency and the relative shift in ε_r'' at each of the indicated temperatures are represented by ●.

To demonstrate this point, the data were reanalyzed with these two highest temperature data points neglected, giving the dashed line in Figure 11a, R^2= 0.9364, A_0 in the range 0.3 – 4 MHz and E_a = 0.15 ± 0.02 eV. Figure 11b presents the same data plotted according to activated tunnelling; this reveals better conformity to a linear relationship (R^2 = 0.9901) and gives values of f_0 = 26.4 ± 0.9 THz and Δ = 0.380 ± 0.002 eV, Table 3.

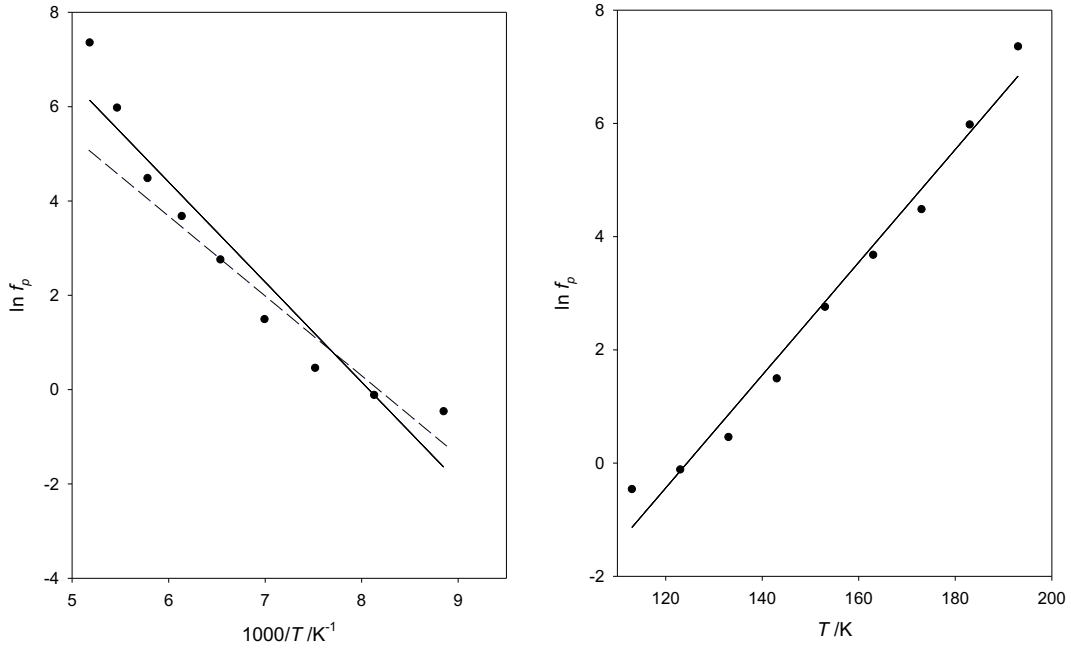

Figure 11. Analysis of the temperature dependence of the 30AGNPE system γ relaxation frequency: (a) Arrhenius plot of lnf_p versus 1/T; (b) activated tunnelling plot of lnf_p versus T.

4. Discussion

The previous section has presented an analysis of the gamma relaxation in four epoxy systems according to two different theories. These four systems are closely related, differing only in the number of FNM moieties introduced and the nature of the FNM. The effect of FNH molar loading level is revealed through consideration of the reference, 20AGHE and 30AGHE sample set; any effects arising from changes in the structure of the FNM at constant molar loading level is revealed by comparison of 30AGHE and 30AGNPE; additionally, the system 20AGHE was chosen for study to provide a material with a comparable T_g to that of 30AGNPE. It is reasonable to expect that such systematic variations in composition/network topology should be reflected in systematic variations in the characteristics of the γ relaxation since, ultimately, this is defined by the structure and molecular composition of the system.

Before comparing the effect of FNM loading and nature upon the γ-relaxation it is necessary to consider further the processes involved in thermal activation and activated tunnelling. Thermal activation considers the probability of a moiety being excited from one state to another over a potential barrier at a temperature T and, as such, the Arrhenius equation is essentially an attempt frequency multiplied by the probability of success, as given by the Boltzmann factor. Activated tunnelling also involves thermal activation to an excited state but, then, considers the possibility of tunnelling through the barrier when excitation occurs to a level below the top of the barrier. As such, activated tunnelling involves two factors: the probability of activation to levels above the ground state that is exponentially reduced by the normal Boltzmann factor; and the tunnelling probability at that level. As the top of the barrier is approached, so the width of the barrier is reduced, thereby exponentially increasingly the probability of tunnelling through it. This leads to the concept of an optimum excitation level, corresponding to an optimum of these two competing factors. Clearly, a condition also exists whereby the optimum excitation level corresponds to thermal activation to the top of the potential barrier, at which point, the activated tunnelling and Arrhenius approaches are effectively equivalent. As such, for the tunnelling component to be significant, activated tunnelling must involve thermal excitation to an excited state within the local potential well that is below the top of the energy barrier; this process is therefore, necessarily limited to low temperatures, whereby the condition of low temperatures is defined by:

$$T < \frac{(7.5\Delta)^{1/2}}{Ad_0k}$$

Thus, as the height of the potential barrier, Δ, decreases so does the temperature range over which activated tunnelling is experimentally distinguishable from Arrhenius behavior. Although the precise form of the above equation is dependent on the shape of the potential barrier, substitution of the estimated parameter values, Table 3, allow the behavior of the different materials to be compared.

First the reference system and 30AGHE are compared. These materials differ in that 30% of the epoxide groups from the DGEBA in the reference system have been substituted with the same number of epoxide groups from the monofunctional GHE. Values for Δ, A and d_0 for the reference epoxy lead to an estimated maximum temperature of applicability of activated tunnelling that is in excess of 500 K. Conversely, for 30AGHE, it is estimated that excitation to the top of the barrier will occur at T ~140 K; how close to 140 K the activated tunnelling expression holds depends upon the detailed dependence of the energy upon position close to the top of the barrier. Nevertheless, it is to be expected that above 140 K both approaches should fit equally well and lead to equivalent derived parameter values, as is found. Furthermore, the Arrhenius expression would be expected to lead to a slightly reduced pre-exponential frequency, due to the reduction of vibration frequencies at and above the energy maxima in a double minima energy well.

Consider now the intermediate composition system, 20AGHE. Comparison of the Arrhenius parameter values obtained from this system with those obtained from the reference and 30AGHE reveals that both the pre-exponential term A_0 and the Arrhenius activation energy, E_a, are intermediate in value, suggesting that both these parameters vary monotonically with composition. Furthermore, as T_g drops progressively from the reference system, through 20AGHE to 30AGHE, so both A_0 and E_a increase. Evaluating, as above, the temperature at which the optimum excitation level reaches the top of

the potential barrier leads to a value of ~210 K, somewhat above the maximum temperature of the reported measurements. This suggests that at the higher temperatures of the measured data the behavior should show some trend away from activated tunnelling towards an Arrhenius behavior which is not evident in Figure 9b. It is possible that the maximum temperature has been underestimated due to assumptions about the shape of the potential surface in the barrier region. Furthermore quantum mechanical tunnelling is probabilistic and thermal activation will occur to a range of different excited states such that it would be expected that activated tunnelling would go smoothly over to Arrhenius behavior and by considering this, we estimate that when the optimum excitation level approaches within 10% of the barrier energy, activation over the barrier will contribute considerably to the overall process. Since such activations result in less than the optimal rate they will contribute to $\varepsilon''(f)$ at frequencies below the peak value and can be expected to result in changes to the shape of the peak. Necessarily, in this region the details of the energy surface become highly influential.

Moving now to 30AGNPE, comparison of the Arrhenius plots and derived parameter values obtained from 20AGHE and 30AGNPE, Table 3, reveals strong similarities. In both 20AGHE and 30AGNPE, the Arrhenius plot exhibits curvature, with an increase in the gradient as $1/T$ diminishes. In both 20AGHE and 30AGNPE, the derived pre-exponential A_0 term falls in the MHz range and, therefore, is intermediate between the kHz value derived from the reference epoxy and the THz value derived from the 30AGHE. In both 20AGHE and 30AGNPE, the derived activation energy, E_a, falls in the range 0.15 – 0.18 eV and therefore, again, is intermediate in magnitude between the values obtained from the reference epoxy and 30AGHE. Furthermore, evaluating the temperature at which the optimum excitation level reaches the top of the barrier in 30AGNPE leads to a value of ~220 K – close to that found in 20AGHE suggesting, again, that in this system the higher part of the temperature range at which the gamma relaxation is readily examined experimentally corresponds to that in which activated tunnelling is going over to thermal activation. To examine this notion further, Arrhenius fits to just the three lowest and three highest temperature data points shown in Figure 11 were evaluated leading, respectively, to A_0 and E_a parameters of A_0 ~0.25 kHz and E_a ~0.06 eV (lowest temperatures) and A_0 ~100 THz and E_a ~0.4 eV (highest temperatures). That is, parameters values that are comparable, respectively, to those determined from Arrhenius fits to the data obtained from the reference system and 30AGHE. Furthermore the Arrhenius activation energy value derived from the highest temperature data (~0.4 eV) is comparable to that obtained from the activated tunnelling analysis of the complete data set (0.380 ± 0.002).

It is evident from a mathematical perspective that, for a single experimental data set, $\ln f_p$ cannot vary linearly with both $1/T$ (Arrhenius equation) and T, as would appear to be the case from Figure 7. If, as we suggest, pure thermal activation, as described by the Arrhenius equation is, in the case of the process considered here, just a manifestation of activated tunnelling above some material dependent temperature, then it is reasonable that (a) all the data sets should exhibit some degree of curvature when plotted in the form of $\ln f_p$ against $1/T$ and (b) that this should be well represented in all materials at all temperatures by activated tunnelling. This is indeed evident in Figure 12, which presents all the experimental data discussed above plotted in the form of $\ln f_p$ against $1/T$ together with the associated fits to the activated tunnelling theory: varying degrees of curvature are evident in all the data sets; this is mirrored in all cases by the relevant activated tunnelling fit.

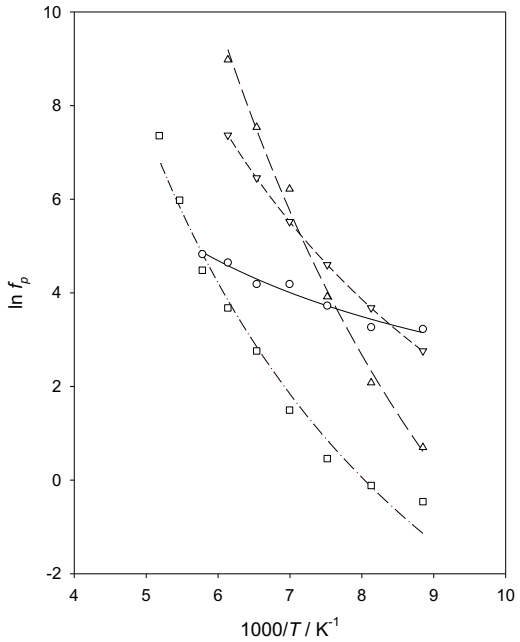

Figure 12. Plots of ln f_p versus 1000/T showing the data for all four material formulations together with the activated tunnelling best fit lines: ○ and solid line, reference epoxy; △ and long dash line, 30AGHE; ▽ and short dash line, 20AGHE; □ and dash dot line, 30AGNPE.

While the molecular origin of the γ relaxation in the materials studied will be covered in detail in a subsequent paper, the parameters of the activated tunnelling model, Table 3, allow us to make some general deductions about the physical nature of the relaxation site. What can be seen is that, Δ, and f_0 increase, and d_0 decreases, for the order of materials, 30AGHE, 20AGHE, 30AGNPE and the reference system. This sequence of parameter values corresponds to an increasing restriction on the re-orienting dipole (tunnelling proton), i.e. the local structure at the dipole site becomes increasingly constrained. This is clearly consistent with the value of T_g which increases in the same order. It is therefore clear that the activated tunnelling model represents an excellent description of the data and one that has a well-founded physical basis.

5. Conclusions

It has been shown that an analysis of the characteristic relaxation frequency of the γ relaxation dielectric loss peak of a related series of epoxy resins in terms of the thermally assisted (activated) tunnelling of a proton at local sites provides a better description of the nature of this relaxation than the traditional Arrhenius theory. In addition to exhibiting a better fit to the data in a number of cases the activated tunnelling parameters provide a physical description of the potential surface of the relaxation site that can be correlated with material topological constraints, as expressed through the glass transition temperature. The maximum temperature for which activated tunnelling can be expected to apply has also been determined and shown to be consistent with the measuring range thereby allowing identification of a material in which activated tunnelling changes to Arrhenius behaviour at the higher temperatures of measurement.

Author Contributions:
Conceptualization, L.A.D. and A.S.V. ; validation, A.S.V. and N.C.; formal analysis, L.A.D. ; Experimental measurements, I.A.S.; writing—review and editing, L.A.D.,A.S.V, I.A.S., N.C, T.A.; Writing—original draft preparation, I.A.S., T.A. and A.S.V.

Acknowledgments: The authors would like to acknowledge the financial support of the Schlumberger Foundation Faculty for the Future.

Conflicts of Interest: The authors declare no conflict of interest.

References

1. W. G. Potter, *Epoxide resins*. London, United Kingdom: The plastics institute, 1970.
2. Neville, K.; Lee, H. Handbook of Epoxy Resins; MacGraw-Hill: New York, NY, USA, 1967
3. J.A. Brydson, Plastics Materials, 7th Edition, Butterworth Heineman, Oxford, 1999.
4. Ellis, B. Chemistry and Technology of Epoxy Resins; Springer: Hall, UK, 1993.
5. Ashcroft, W. R. In Chemistry and Technology of Epoxy Resins Springer Netherlands 1993; pp. 37–71.
6. C. May, *Epoxy resins: chemistry and technology*: CRC press, 1987.
7. G. C. Stevens, "Cure kinetics of a low epoxide/hydroxyl group-ratio bisphenol a epoxy resin–anhydride system by infrared absorption spectroscopy," *Journal of Applied Polymer Science,* vol. 26, pp. 4259-4278, 1981.
8. C. Wang and C. Kwag, "Cure kinetics of an epoxy-anhydride-imidazole resin system by isothermal DSC," *Polymers and Polymer Composites,* vol. 14, pp. 445-454, 2006.
9. W. H. Park and J. K. Lee, "A study on isothermal cure behavior of an epoxy-rich/anhydride system by differential scanning calorimetry," *Journal of applied polymer science,* vol. 67, pp. 1101-1108, 1998.
10. F. Kolar and J. Svitilova, "Kinetics and mechanism of curing epoxy/anhydride systems," *Acta Geodynamica et Geromaterialia,* vol. 4, pp. 85-93, 2007.
11. S. Montserrat, C. Flaque, M. Calafell, G. Andreu, and J. Malek, "Influence of the accelerator concentration on the curing reaction of an epoxy-anhydride system," *Thermochimica Acta,* vol. 269, pp. 213-229, 1995.
12. Harani, H.; Fellahi, S.; Bakar, M. Toughening of epoxy resin using hydroxyl-terminated polyesters. J. Appl. Polym. Sci. 1999, 71, 29–38.
13. Tang, B.; Liu, X.; Zhao, X.; Zhang, J. Highly efficient in situ toughening of epoxy thermosets with reactive hyperbranched polyurethane. J. Appl. Polym. Sci. 2014, 131, 40614.
14. Gui, D.; Gao, X.; Hao, J.; Liu, J. Preparation and characterization of liquid crystalline polyurethane-imide modified epoxy resin composites. Polym. Eng. Sci. 2014, 54, 1704–1711.
15. F. N. Alhabill, R. Ayoob, T. Andritsch and A. S. Vaughan, Effect of Resin/Hardener Stoichiometry on Electrical Behavior of Epoxy Networks, IEEE Trans. Diel. Electr. Insul., 24 (6), 2017, pp. 3739-3749.
16. V. T. Nguyen, A. S. Vaughan, P. L. Lewin, and A. Krivda, The Effect of Resin Stoichiometry and Nanoparticle Addition on Epoxy/Silica Nanodielectrics, IEEE Trans. Diel. Electr. Insul., 22 (2), 2015 pp. 895-905
17. I.A. Saeedi, A.S. Vaughan and T. Andritsch, Functional design of epoxy-based networks: tailoring advanced dielectrics for next-generation energy systems, J. Phys. D: Appl. Phys. 52 (2019) 205301 (11pp)
18. I.A. Saeedi, S. Chaudhary, T. Andritsch and A.S. Vaughan, Investigation of the Functional Network Modifier Loading on the Stoichiometric Ratio of Epoxy Resins and their Dielectric Properties, J. Mater. Sci, in press 2021.
19. Hammerton, I. Recent Developments in Epoxy Resins (Rapra Review Reports); Smithers Rapra Technology:Shrewsbury, UK, 1997.
20. M. Beiner and K. Ngai, "Interrelation between primary and secondary relaxations in polymerizing systems based on epoxy resins," *Macromolecules,* vol. 38, pp. 7033-7042, 2005. doi:10.1021/ma050384j
21. E. Crawford and A. J. Lesser, "The effect of network architecture on the thermal and mechanical behavior of epoxy resins," *Journal of Polymer Science Part B: Polymer Physics,* vol. 36, pp. 1371-1382, 1998.
22. K. Ngai, "Relation between some secondary relaxations and the α relaxations in glass-forming materials according to the coupling model," *The Journal of chemical physics,* vol. 109, pp. 6982-6994, 1998.
23. F. Kremer and A. Schönhals, Broadband Dielectric Spectroscopy: Springer Berlin Heidelberg, 2012.
24. M. K. Hassan, S. J. Tucker, A. Abukmail, J. S. Wiggins, and K. A. Mauritz, "Polymer chain dynamics in epoxy based composites as investigated by broadband dielectric spectroscopy," Arabian Journal of Chemistry, vol. 9, pp. 305-315, 2016.
25. H. Hammami, M. Arous, M. Lagache, and A. Kallel, "Study of the interfacial MWS relaxation by dielectric spectroscopy in unidirectional PZT fibres/epoxy resin composites," Journal of alloys and compounds, vol. 430, pp. 1-8, 2007.
26. M.B.M. Mangion, G.P. Johari, Relaxations of thermosets. III. Sub-Tg dielectric relaxations of bisphenol-A–based epoxide cured with different cross-linking agents, J. Polym. Sci. Part B Polym. Phys. 28 (1990) 71–83. doi:10.1002/polb.1990.090280106.
27. B. Fitz, S. Andjelić, J. Mijović, Reorientational Dynamics and Intermolecular Cooperativity of Reactive Polymers. 1. Model Epoxy-Amine Systems, Macromolecules. 30 (1997) 5227–5238. doi:10.1021/ma970010t.
28. E. Butta, A. Livi, G. Levita, P.A. Rolla, Dielectric analysis of an epoxy resin during cross-linking, J. Polym. Sci. Part B Polym. Phys. 33 (1995) 2253–2261. doi:10.1002/polb.1995.090331610.
29. F. Román, P. Colomer, Y. Calventus, J.M. Hutchinson, Molecular mobility in hyperbranched polymers and their interaction with an epoxy matrix, Materials (Basel). 9 (2016) 1–26. doi:10.3390/ma9030192.
30. S. Andjelić, B. Fitz, J. Mijović, Reorientational dynamics and intermolecular cooperativity in reactive polymers. 2. Multifunctional epoxy-amine systems, Macromolecules. 30 (1997) 5239–5248. doi:10.1021/ma970010t.
31. J. Mijović, H. Zhang, Local dynamics and molecular origin of polymer network-water interactions as studied by broadband dielectric relaxation spectroscopy, FTIR, and molecular simulations, Macromolecules. 36 (2003) 1279–1288. doi:10.1021/ma021568q.
32. S. Cukierman, J. -L Halary, L. Monnerie, Dynamic mechanical response of model epoxy networks in the glassy state, Polym. Eng. Sci. 31 (1991) 1476–1482. doi:10.1002/pen.760312006.
33. T.D. Chang, S.H. Carr, J.O. Brittain, Studies of epoxy resin systems: Part A: A study of the origins of the secondary relaxations of epoxy resins by thermally stimulated depolarization, Polym. Eng. Sci. 22 (1982) 1205–1212. doi:10.1002/pen.760221806.

34. G.A. Kontos, A.L. Soulintzis, P.K. Karahaliou, G.C. Psarras, S.N. Georga, C.A. Krontiras, M.N. Pisanias, Electrical relaxation dynamics in TiO2 - polymer matrix composites, Express Polym. Lett. 1 (2007) 781–789. doi:10.3144/expresspolymlett.2007.108.
35. S. Pangrle, C.S. Wu, P.H. Geil, Low temperature relaxation of DGEBA epoxy resins: A thermally stimulated discharge current (TSDC) study, Polym. Compos. 10 (1989) 173–183. doi:10.1002/pc.750100305.
36. M. Ochi, O. Masatoshi, M. Shimbo, Mechanical Relaxation of Epoxide Resins Cured with Amines, J. Polym. Sci. Polym. Phys. Ed. 20 (1982) 689–699. doi:10.1246/nikkashi.1976.1004.
37. J.M. Charlesworth, Effect of crosslink density on the molecular relaxations in diepoxide-diamine network polymers. Part 1. The glassy region, Polym. Eng. Sci. 28 (1988) 221–229. doi:10.1002/pen.760280405.
38. O. Vryonis, S. Riarh, T. Andritsch, A.S. Vaughan, Stoichiometry and molecular dynamics of anhydride-cured epoxy resin incorporating octa-glycidyl POSS Co-Monomer, Polymer, 213, 2021, Article Number: 123312
39. I.A. Saeedi, 2021. *Dielectric properties of modified epoxy resin systems: A novel approach for developing materials for new generation technologies*. Doctorate of philosophy. University of Southampton.
40. Y. Liu, A. S. Vaughan, I. L. Hosier, C. Yeung, and T. Andritsch, “On epoxy network structure and dielectric performance,” in Electrical Insulation and Dielectric Phenomena (CEIDP), IEEE Conference, 2015, pp. 114–117.
41. P. G. Babayevsky and J. Gillham, “Epoxy thermosetting systems: dynamic mechanical analysis of the reactions of aromatic diamines with the diglycidyl ether of bisphenol a,” Journal of Applied Polymer Science, vol. 17, no. 7, pp. 2067–2088, 1973.
42. A. Soulintzis, G. Kontos, P. Karahaliou, G.C. Psarras, S.N. Georga, C.A. Krontiras, Dielectric Relaxation Processes in Epoxy Resin-ZnO Composites, JOURNAL OF POLYMER SCIENCE PART B-POLYMER PHYSICS, Volume: 47 Issue: 4 Pages: 445-454 DOI: 10.1002/polb.21649 Published: FEB 15 2009
43. I.A. Saeedi, T. Andritsch, A.S. Vaughan, On the Dielectric Behavior of Amine and Anhydride Cured Epoxy Resins Modified Using Multi-Terminal Epoxy Functional Network Modifier, POLYMERS, Volume: 11 Issue: 8, Article Number: 1271, DOI: 10.3390/polym11081271, Published: AUG 2019
44. S. Corezzi, M. Beiner, H. Huth, K. Schröter, S. Capaccioli, R. Casalini, D. Fioretto, E. Donth, Two crossover regions in the dynamics of glass forming epoxy resins, J. Chem. Phys. 117 (2002) 2435–2448. doi:10.1063/1.1486214.
45. F.R. Dammont, T.K. Kwei, Low-Temperature Dispersion Related to Methylene Units of a Polymer Main Chain, J. Polym. Sci. Part A-2 Polym. Phys. 6 (1968) 457–462
46. R M Hill and L A Dissado, The temperature dependence of relaxation processes 1982 J. Phys. C: Solid State Phys. 15 5171-5193